Dyadic Green's Functions for Dipole Excitation of Homogenized Metasurfaces

Feng Liang, George W. Hanson, *Fellow, IEEE*, Alexander B. Yakovlev, *Senior Member, IEEE*, Giampiero Lovat, *Member, IEEE*, Paolo Burghignoli, *Senior Member, IEEE*, Rodolfo Araneo, *Senior Member, IEEE*, and Seyyed Ali Hassani Gangaraj, *Student Member, IEEE*

***Abstract*—Dyadic Green's functions for an electric dipole source over an infinite periodic metasurface are obtained using homogenized, nonlocal, anisotropic, generalized sheet-transition conditions. The homogenized Green's functions can efficiently model near-field point source excitation of typical metasurface structures. The Green's functions can be decomposed into discrete and continuous spectral components, providing physical insight into the wave dynamics. Several different metasurfaces are considered, and the results are validated by comparison with a full-wave array-scanning method, demonstrating computational efficiency of the proposed homogenized Green's function approach.**

***Index Terms*—Green's functions, homogenization, metasurface.**

I. Introduction

METASURFACES are single-layer, electrically thin metamaterial structures that have been attracting growing interest in recent years among researchers in microwave [1]–[3], terahertz [4], [5], and optical [6]–[8] communities. Metasurfaces possess extraordinary capabilities to manipulate wavefronts and control polarization, reflection and transmission characteristics, and beam-forming [6]–[11]. Wavefront manipulation has also been shown to be promising with Huygens metasurfaces [12], [13]. Due to the subwavelength nature of metasurfaces, low loss compared to bulk materials, and capabilities of modifying propagating and radiating characteristics, they find potential applications in radio frequency, optical, and biomedical devices [1].

It has been shown that finite-thickness effective medium models of metasurfaces are inappropriate [14]. Here, we follow in part Holloway and Kuester [15] and model a metasurface as a two-dimensional (2-D) surface with equivalent electric and magnetic susceptibility dyadics and generalized sheet-transition conditions (GSTCs). Although considerable attention has been given to the plane-wave problem [16]–[18], much less work has been done on the near-field excitation (homogenized Green's functions) of metasurfaces, although the problem of line-source excitation of a metasurface modeled by susceptibilities has been presented in [2].

Another 2-D representation of a metasurface is in terms of homogenized surface impedances [19], [20]. Here also, most attention has been given to the plane wave problem [21]–[24], although homogenized Green's functions for line-source excitations were presented in [25], and previously for one-dimensional (1-D) periodic structures, in [26]. Thus, all previous works on homogenized Green's functions, either using susceptibility dyadics or surface impedances, have been done assuming a line-source excitation.

In this paper, we present homogenized dyadic Green's functions for a point source near an anisotropic metasurface, using both the susceptibility dyadic and the surface-impedance approach. Both methods result in nonlocal anisotropic sheet-transition conditions and lead to the Green's function in quasi-analytical (Sommerfeld integral) form. This provides physical insight into the wave dynamics, e.g., identifying surface-wave propagation and allowing the field to be decomposed in terms of discrete and continuous spectra. Results are compared to those obtained using a full-wave method of moments in conjunction with the array-scanning method (ASM-MoM) [27]–[29]. It should be noted that the ASM is quite specialized, and not implemented in any commercial code, and so a commercial simulator cannot model these structures (periodic surfaces with a single source—if one uses periodic boundary conditions in a commercial code, the source is also made periodic). The only alternative in a commercial code is to model a finite structure consisting of a sufficiently large number of unit cells, which is extremely time-consuming. Also, often commercial simulators are inaccurate when the source point is close to the observation point. As such, the method presented here is computationally much more efficient than full-wave methods, and the homogenized Green's functions are found to be accurate when the

Manuscript received June 05, 2015; revised November 11, 2015; accepted November 13, 2015. Date of publication November 18, 2015; date of current version December 31, 2015. This work was supported in part by the National Natural Science Foundation of China under Grant 61204041, in part by the China Postdoctoral Science Foundation under Grant 2014M552335, in part by the Fundamental Research Funds for the Central Universities of China under Grant ZYGX2013J049, and the China Scholarship Council.

F. Liang is with the School of Physical Electronics, University of Electronic Science and Technology of China, Chengdu 610054, China (e-mail: fengliang@uestc.edu.cn).

G. W. Hanson and S. A. Hassani Gangaraj are with the Department of Electrical Engineering, University of Wisconsin-Milwaukee, Milwaukee, WI 53211 USA (e-mail: george@uwm.edu).

A. B. Yakovlev is with the Department of Electrical Engineering, The University of Mississippi, University, MS 38677 USA (e-mail: yakovlev@olemiss.edu).

G. Lovat and R. Araneo are with the Department of Astronautic, Electrical and Energetic Engineering, "La Sapienza" University of Rome, 00184 Rome, Italy (e-mail: giampiero.lovat@uniroma1.it; rodolfo.araneo@uniroma1.it).

P. Burghignoli is with the Department of Information Engineering, Electronics and Telecommunications, "La Sapienza" University of Rome, 00184 Rome, Italy (e-mail: burghignoli@die.uniroma1.it).

Color versions of one or more of the figures in this paper are available online at http://ieeexplore.ieee.org.

Digital Object Identifier 10.1109/TAP.2015.2501430

homogenization is valid (period small compared to wavelength) except for points extremely close to the surface (less than a period). Although recent work on metasurfaces mainly considers structures with inhomogeneous (nonperiodic) surface properties, we point out toward the end of the paper a potential application of controllable surface-wave excitation on an infinite periodic graphene metasurface, which can be analyzed using our efficient method.

II. General Dyadic Green's Functions

Consider a metasurface represented by an equivalent homogenized 2-D surface with electric conductivity tensor $\underline{\boldsymbol{\sigma}}_e$ and magnetic conductivity tensor $\underline{\boldsymbol{\sigma}}_m$. We will initially assume that the metasurface is at the interface of two half-spaces, as shown in Fig. 1(a); later we will consider layered media. A dipole source is above the surface in region 1, with region 2 being below the surface. The electric field can be written as (time-dependence $e^{j\omega t}$)

$$\mathbf{E}^{(n)}(\mathbf{r}) = -j\omega\mu \int_{\Omega} \underline{\mathbf{G}}_e^{(n)}(\mathbf{r},\mathbf{r}') \cdot \mathbf{J}(\mathbf{r}')\, d\Omega' \tag{1}$$

$$\mathbf{H}^{(n)}(\mathbf{r}) = \int_{\Omega} \nabla \times \underline{\mathbf{G}}_e^{(n)}(\mathbf{r},\mathbf{r}') \cdot \mathbf{J}(\mathbf{r}')\, d\Omega' \tag{2}$$

where $\underline{\mathbf{G}}_e^{(1)} = \underline{\mathbf{G}}_0^{(1)} + \underline{\mathbf{G}}_r^{(1)}, \underline{\mathbf{G}}_e^{(2)} = \underline{\mathbf{G}}_t^{(2)}$

$$\underline{\mathbf{G}}_0^{(1)} = \left(\underline{\mathbf{I}} + \frac{\nabla\nabla}{k_1^2}\right) g, g = \frac{e^{-jk_1 R}}{4\pi R} \tag{3}$$

and $R = |\mathbf{r} - \mathbf{r}'|$. The scattered (reflected and transmitted) Green's functions are [30], [31]

$$\begin{aligned}\underline{\mathbf{G}}_r^{(1)} = \frac{-j}{8\pi^2} \iint \frac{1}{k_{1z}} \big(& r_{tt}\hat{\mathbf{t}}_1^+\hat{\mathbf{t}}_1^- + r_{tp}\hat{\mathbf{t}}_1^+\hat{\mathbf{p}}_1^- + r_{pt}\hat{\mathbf{p}}_1^+\hat{\mathbf{t}}_1^- \\ &+ r_{pp}\hat{\mathbf{p}}_1^+\hat{\mathbf{p}}_1^-\big) e^{-j\mathbf{k}_1^+\cdot\mathbf{r}} e^{j\mathbf{k}_1^-\cdot\mathbf{r}'} dk_x dk_y \end{aligned} \tag{4}$$

$$\begin{aligned}\underline{\mathbf{G}}_t^{(2)} = \frac{-j}{8\pi^2} \iint \frac{1}{k_{1z}} \big(& t_{tt}\hat{\mathbf{t}}_2^-\hat{\mathbf{t}}_1^- + t_{tp}\hat{\mathbf{t}}_2^-\hat{\mathbf{p}}_1^- + t_{pt}\hat{\mathbf{p}}_2^-\hat{\mathbf{t}}_1^- \\ &+ t_{pp}\hat{\mathbf{p}}_2^-\hat{\mathbf{p}}_1^-\big) e^{-j\mathbf{k}_2^-\cdot\mathbf{r}} e^{j\mathbf{k}_1^-\cdot\mathbf{r}'} dk_x dk_y \end{aligned} \tag{5}$$

where $\mathbf{k}_n^\pm = \hat{\mathbf{x}}k_x + \hat{\mathbf{y}}k_y \pm \hat{\mathbf{z}}k_{nz}$ and $k_{nz} = \sqrt{k_n^2 - k_x^2 - k_y^2}$, such that $\hat{\mathbf{k}}_n^\pm = \frac{1}{k_n}(\hat{\mathbf{x}}k_x + \hat{\mathbf{y}}k_y \pm \hat{\mathbf{z}}k_{nz})$, $k_n = |\mathbf{k}_n^\pm|$, and

$$\hat{\mathbf{t}}_n^\pm = \frac{\hat{\mathbf{z}} \times \hat{\mathbf{k}}_n^\pm}{\left|\hat{\mathbf{z}} \times \hat{\mathbf{k}}_n^\pm\right|}, \hat{\mathbf{p}}_n^\pm = \hat{\mathbf{k}}_n^\pm \times \hat{\mathbf{t}}_n^\pm. \tag{6}$$

The tensor boundary conditions (i.e., GTSCs) in the tangential transform domain (k_x, k_y, z) are [1]

$$\hat{\mathbf{z}} \times \left(\mathbf{H}^{(1)} - \mathbf{H}^{(2)}\right) = \frac{1}{2}\underline{\boldsymbol{\sigma}}_e \cdot \left(\mathbf{E}_T^{(1)} + \mathbf{E}_T^{(2)}\right) \tag{7}$$

$$-\hat{\mathbf{z}} \times \left(\mathbf{E}^{(1)} - \mathbf{E}^{(2)}\right) = \frac{1}{2}\underline{\boldsymbol{\sigma}}_m \cdot \left(\mathbf{H}_T^{(1)} + \mathbf{H}_T^{(2)}\right) \tag{8}$$

where the subscript T denotes the tangential components, and where the nonlocal material tensors are defined below. Applying the boundary conditions, the coefficients $r_{\alpha\beta}$ and $t_{\alpha\beta}$ (where $\alpha = t$ or p, $\beta = t$ or p) can be obtained by solving eight linear equations. Assuming the special case $k_1 = k_2 = k$ and $k_{1z} = k_{2z} = k_z$ leads to greatly simplified coefficients, and in the following, we will assume this condition, writing simply k and k_z.

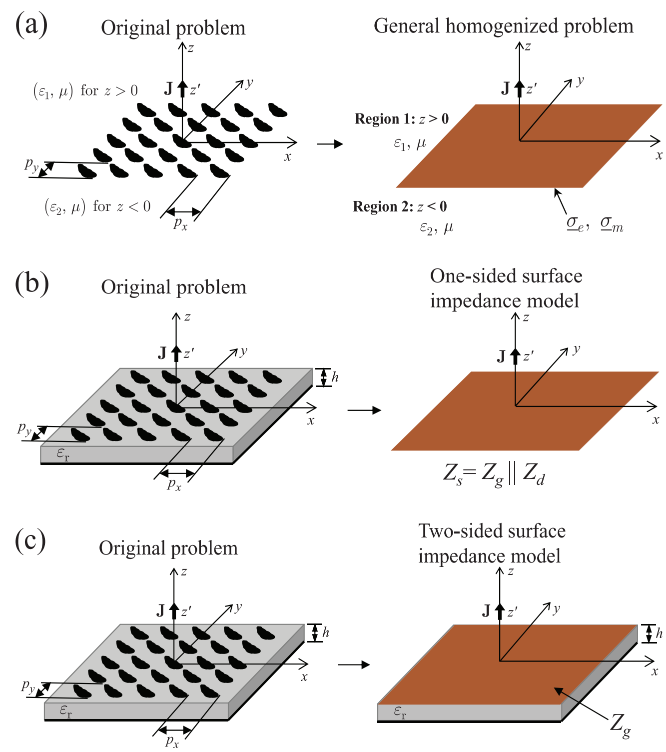

Fig. 1. Original problem and its equivalent homogenized problem represented by (a) general sheet with electric conductivity tensor $\underline{\boldsymbol{\sigma}}_e$ and magnetic conductivity tensor $\underline{\boldsymbol{\sigma}}_m$; (b) one-sided impedance surface; and (c) two-sided impedance surface.

The generally nonlocal electric and magnetic conductivity tensors $\underline{\boldsymbol{\sigma}}_e$ and $\underline{\boldsymbol{\sigma}}_m$ can be expressed in terms of susceptibilities [1], [14], [15], [18], [32] or surface impedances [20], [25]. Which method is more convenient to use depends on which characterization of the subwavelength objects is available. For simple objects, one can obtain both the surface susceptibilities and the surface-impedance values in a simple closed form (e.g., for metal patches, the susceptibilities are available in [32] and [33], and the surface-impedance values in [20] and [25]). For more complicated unit cells, [1] and references therein provide a means of obtaining the surface susceptibilities from full-wave numerical computation. In the following, we will use both the susceptibility and the surface-impedance methods for a metasurface in a homogeneous host medium [see Fig. 1(a), with $\varepsilon_1 = \varepsilon_2$]. For a metasurface over a layered medium [e.g., Figs. 1(b) and (c)], it is more convenient to use the surface-impedance method.

A. Susceptibility Method

Representing the equivalent electric and magnetic conductivity tensors in terms of susceptibilities leads to the nonlocal dispersive tensors [1]

$$\underline{\boldsymbol{\sigma}}_e(\omega,\mathbf{k}) = \underline{\boldsymbol{\sigma}}_e = j\omega\varepsilon\underline{\chi}_{ES} + \frac{j\chi_{MS}^{zz}}{\omega\mu}(\hat{\mathbf{z}}\times\mathbf{k})(\hat{\mathbf{z}}\times\mathbf{k}) \quad (9)$$

$$\underline{\boldsymbol{\sigma}}_m(\omega,\mathbf{k}) = \underline{\boldsymbol{\sigma}}_m = j\omega\mu\underline{\chi}_{MS} + \frac{j\chi_{ES}^{zz}}{\omega\varepsilon}(\hat{\mathbf{z}}\times\mathbf{k})(\hat{\mathbf{z}}\times\mathbf{k}) \quad (10)$$

where $\underline{\chi}_{ES} = \hat{\mathbf{x}}\hat{\mathbf{x}}\chi_{ES}^{xx} + \hat{\mathbf{y}}\hat{\mathbf{y}}\chi_{ES}^{yy} + \hat{\mathbf{z}}\hat{\mathbf{z}}\chi_{ES}^{zz}$ and $\underline{\chi}_{MS} = \hat{\mathbf{x}}\hat{\mathbf{x}}\chi_{MS}^{xx} + \hat{\mathbf{y}}\hat{\mathbf{y}}\chi_{MS}^{yy} + \hat{\mathbf{z}}\hat{\mathbf{z}}\chi_{MS}^{zz}$ are the surface electric and magnetic susceptibility dyadics, respectively, assumed to be diagonal in the xyz reference frame.

The Green's function coefficients $r_{\alpha\beta}$ and $t_{\alpha\beta}$ in the general case are extremely complicated. However, when $\chi_{ES}^{yy} = \chi_{ES}^{xx}$ and $\chi_{MS}^{yy} = \chi_{MS}^{xx}$ (valid when the physical structure is symmetric in the x and y directions), these coefficients reduce to [2]

$$r_{tt} = \frac{2j\left(k^2\chi_{ES}^{xx} - k_z^2\chi_{MS}^{xx} + k_T^2\chi_{MS}^{zz}\right)}{\left(k^2\chi_{ES}^{xx} + k_T^2\chi_{MS}^{zz} - 2jk_z\right)\left(k_z\chi_{MS}^{xx} - 2j\right)} \quad (11)$$

$$t_{tt} = \frac{-k_z\left[4 + \chi_{MS}^{xx}\left(k^2\chi_{ES}^{xx} + k_T^2\chi_{MS}^{zz}\right)\right]}{\left(k^2\chi_{ES}^{xx} + k_T^2\chi_{MS}^{zz} - 2jk_z\right)\left(k_z\chi_{MS}^{xx} - 2j\right)} \quad (12)$$

with r_{pp} and t_{pp} obtained by replacing (ES, MS) with (MS, ES) in (11) and (12), respectively, and $r_{tp} = r_{pt} = t_{tp} = t_{pt} = 0$, where $k_T = \sqrt{k_x^2 + k_y^2}$ is the tangential wavenumber.

B. Surface-Impedance Method

As an alternative to the polarizability/surface-susceptibility method, a planar metasurface can be modeled in terms of a one-sided or two-sided surface-impedance condition. In general, the two-sided surface-impedance method and the susceptibility method can be made equivalent to each other if the impedances are defined in terms of the susceptibilities, see e.g., (6) in [1]. Here, we assume that there is no magnetic response ($\underline{\boldsymbol{\sigma}}_m$), which is valid for strictly planar geometries (e.g., an array of spheres would lead to $\underline{\boldsymbol{\sigma}}_m \neq 0$), and we consider unit cells for which TE-TM coupling is absent or negligible.

1) Method I One-Sided Surface Impedance: This method makes it particularly convenient to account for multiple planar layers below the metasurface. In this method, the boundary conditions (7) and (8) reduce to

$$\hat{\mathbf{z}}\times\mathbf{H}^{(1)} = \underline{\boldsymbol{\sigma}}_e\cdot\mathbf{E}_T{}^{(1)} \quad (13)$$

where $\underline{\boldsymbol{\sigma}}_e = \underline{\mathbf{Z}}_s^{-1}$ and $\underline{\mathbf{Z}}_s$ is the nonlocal surface-impedance tensor. For a planar metasurface with square periodic elements, one has [34]

$$\begin{aligned}\underline{\sigma}_e =& K\left[\left(Z_s^{TE}k_x^2 + Z_s^{TM}k_y^2\right)\hat{x}\hat{x} + \left(Z_s^{TM}k_x^2 + Z_s^{TE}k_y^2\right)\hat{y}\hat{y}\right.\\ &\left. + \left(Z_s^{TE} - Z_s^{TM}\right)k_xk_y\left(\hat{x}\hat{y} + \hat{y}\hat{x}\right)\right] \quad (14)\end{aligned}$$

where $K = 1/(Z_s^{TE}Z_s^{TM}k_T^2)$, Z_s^{TE}, and Z_s^{TM} represent the parallel connection of the grid impedance Z_g of the metallization pattern and the input impedance of the region below the surface. Referring to Fig. 1(b), the latter is the input impedance Z_d of the grounded dielectric, so that $Z_s = Z_g \| Z_d$ (where $\|$ indicates a parallel connection), or, considering Fig. 1(a), this is the input impedance of the dielectric half space (for free space, Z_0, such that $Z_s = Z_g \| Z_0$). The expressions for Z_g and Z_d (dependent on the dielectric height, h) can be found in [20] and [25] with replacement of k_x with k_T. The coefficients in the Green's functions can be obtained as

$$r_{tt} = \frac{k_zZ_s^{TE} - \omega\mu}{k_zZ_s^{TE} + \omega\mu},\ r_{pp} = \frac{k^2Z_s^{TM} - \omega\mu k_z}{k^2Z_s^{TM} + \omega\mu k_z} \quad (15)$$

and $r_{tp} = r_{pt} = 0$.

2) Method II: Two-Sided Surface Impedance: In this method, fields can be partially reflected from and transmitted through the metasurface. For the grounded dielectric geometry shown in Fig. 1(c), the boundary conditions (7) and (8) reduce to

$$\hat{\mathbf{z}}\times\left(\mathbf{H}^{(1)} - \mathbf{H}^{(2)}\right) = \frac{1}{2}\underline{\boldsymbol{\sigma}}_e\cdot\left(\mathbf{E}_T^{(1)} + \mathbf{E}_T^{(2)}\right) \quad (16)$$

$$\hat{\mathbf{z}}\times\left(\mathbf{E}^{(1)} - \mathbf{E}^{(2)}\right) = 0 \quad (17)$$

at the metasurface, and

$$\hat{\mathbf{z}}\times\mathbf{E}^{(2)} = 0 \quad (18)$$

at the ground plane, where $\underline{\boldsymbol{\sigma}}_e = \underline{\mathbf{Z}}_g^{-1}$ and $\underline{\mathbf{Z}}_g$ is the grid impedance tensor. For a planar metasurface with square periodic elements, we obtain the expression of $\underline{\mathbf{Z}}_g$ and $\underline{\boldsymbol{\sigma}}_e$ by replacing subscript "s" by "g" in (14). The expressions for the grid impedance Z_g^{TE} and Z_g^{TM} for typical metallization patterns can be found in [20] and [25] by replacement of k_x with k_T. For the special case of a metasurface in a homogeneous medium, the coefficients are

$$r_{tt} = \frac{-\omega\mu}{2k_zZ_g^{TE} + \omega\mu},\ r_{pp} = \frac{\omega\mu k_z}{2k^2Z_g^{TM} + \omega\mu k_z} \quad (19)$$

$$t_{tt} = \frac{2k_zZ_g^{TE}}{2k_zZ_g^{TE} + \omega\mu},\ t_{pp} = \frac{2k^2Z_g^{TM}}{2k^2Z_g^{TM} + \omega\mu k_z} \quad (20)$$

and $r_{tp} = r_{pt} = t_{tp} = t_{pt} = 0$.

When applied to the same geometry, these one-sided and two-sided surface-impedance methods lead to identical results, as shown in [25] for the line-source case. To calculate the fields in the region of the source position (region 1 in Fig. 1), one can choose either the one-sided or two-sided surface-impedance method. When calculating the transmitted fields through the metasurface structure, one needs to use the two-sided surface-impedance method.

III. Electric Dipole Excitation

The formulations in Section II can be applied to arbitrary electric current source excitations. For electric dipole excitations, these formulations can be further simplified. Here, we will consider both vertical electric dipole (VED) and horizontal electric dipole (HED) excitations having unit amplitude (i.e., a 1 A source). In general, for anisotropic and nonlocal materials modeled by (9) and (10), the Green's function is computed as a 2-D integral over tangential wavenumbers. For the isotropic case [starting with (11) and (12)], the spectral integrals can be reduced to one-dimension as shown as follows.

A. VED Source Excitation

For a vertical electric point source $\mathbf{J} = \hat{\mathbf{z}}\delta\left(x - x'\right)\delta\left(y - y'\right)\delta\left(z - z'\right)$, we obtain the z-component of electric field in the same half-space as

$$E_z = -j\omega\mu\left(G_{0,zz} + G_{r,zz}\right) \tag{21}$$

where

$$G_{r,zz} = \frac{-j}{4\pi}\int_0^\infty \frac{r_{pp}k_T^3}{k^2k_z}J_0\left(k_T\rho\right)e^{-jk_z\left(z+z'\right)}dk_T \tag{22}$$

$G_{0,zz} = g + (1/k^2)\partial^2 g/\partial z^2$ and $\rho = \sqrt{\left(x - x'\right)^2 + \left(y - y'\right)^2}$. The scattered field can be decomposed (exactly) into residue (surface wave) and branch-cut (radiation continuum) components as

$$G_{r,zz} = G_{r,zz}^{\mathrm{res}} + G_{r,zz}^{\mathrm{bc}} \tag{23}$$

where the residue field is

$$G_{r,zz}^{\mathrm{res}} = \frac{-1}{4}\sum_{i=1}^{n}\frac{r_{pp}'k_T^3}{k^2k_z}H_0^{(2)}(k_T\rho)e^{-jk_z\left(z+z'\right)}\bigg|_{k_T=k_{T,i}} \tag{24}$$

with

$$r_{pp}' = \frac{N_{r_{pp}}}{\partial D_{r_{pp}}/\partial k_T} \tag{25}$$

where $k_{T,i}$ is the ith pole of r_{pp} that supports surface-wave propagation, and $N_{r_{pp}}$ and $D_{r_{pp}}$ are the numerator and denominator of r_{pp}, respectively. The branch-cut (radiation continuum) contribution is

$$G_{r,zz}^{\mathrm{bc}} = \frac{-j}{8\pi}\int_{\Gamma_{bc}}\frac{r_{pp}k_T^3}{k^2k_z}H_0^{(2)}(k_T\rho)e^{-jk_z\left(z+z'\right)}dk_T \tag{26}$$

where the branch-cut integration is performed over the usual hyperbolic Sommerfeld branch-cuts [35].

B. HED Source Excitation

For a horizontal electric point source $\mathbf{J} = \hat{\mathbf{y}}\delta\left(x - x'\right)\delta\left(y - y'\right)\delta\left(z - z'\right)$, we consider the y-component of scattered electric field in the same half-space

$$G_{r,yy} = \frac{-j}{4\pi}\int_0^\infty\left(\frac{r_{tt}f_{tt}}{k_z} - \frac{r_{pp}k_zf_{pp}}{k^2}\right)k_Te^{-jk_z\left(z+z'\right)}dk_T \tag{27}$$

where

$$f_{tt} = \left(\sin^2\phi - \cos^2\phi\right)J_0''\left(k_T\rho\right) + \sin^2\phi J_0\left(k_T\rho\right) \tag{28}$$

$$f_{pp} = \left(\cos^2\phi - \sin^2\phi\right)J_0''\left(k_T\rho\right) + \cos^2\phi J_0\left(k_T\rho\right) \tag{29}$$

$\phi = \tan^{-1}\left[\left(y - y'\right)/\left(x - x'\right)\right]$, and $J_0''(k_T\rho) = d^2J_0(k_T\rho)/d(k_T\rho)^2$.

To decompose the total field into residue and branch-cut components, (27) can be rewritten as

$$G_{r,yy} = \frac{-j}{8\pi}\int_{-\infty}^\infty\left(\frac{r_{tt}h_{tt}}{k_z} - \frac{r_{pp}k_zh_{pp}}{k^2}\right)k_Te^{-jk_z\left(z+z'\right)}dk_T \tag{30}$$

where

$$h_{tt} = \left(\sin^2\phi - \cos^2\phi\right)\frac{H_1^{(2)}\left(k_T\rho\right)}{k_T\rho} + \cos^2\phi H_0^{(2)}\left(k_T\rho\right) \tag{31}$$

$$h_{pp} = \left(\cos^2\phi - \sin^2\phi\right)\frac{H_1^{(2)}\left(k_T\rho\right)}{k_T\rho} + \sin^2\phi H_0^{(2)}\left(k_T\rho\right). \tag{32}$$

Then

$$G_{r,yy} = G_{r,yy}^{\mathrm{res}} + G_{r,yy}^{\mathrm{bc}} \tag{33}$$

where the residue field is

$$\begin{aligned} G_{r,yy}^{\mathrm{res}} =& \frac{-1}{4}\sum_{i=1}^{n}\frac{r_{tt}'h_{tt}}{k_z}k_Te^{-jk_z\left(z+z'\right)}\bigg|_{k_T=k_{T,i}} \\ &- \frac{1}{4}\sum_{j=1}^{n}\frac{r_{pp}'k_zh_{pp}}{k^2}k_Te^{-jk_z\left(z+z'\right)}\bigg|_{k_T=k_{T,j}} \end{aligned} \tag{34}$$

with

$$r_{tt}' = \frac{N_{r_{tt}}}{\partial D_{r_{tt}}/\partial k_T} \tag{35}$$

where $k_{T,i}$ is the ith pole of r_{tt} that supports surface-wave propagation, $k_{T,j}$ is the jth pole of r_{pp}, and $N_{r_{tt}}$ and $D_{r_{tt}}$ are the numerator and denominator of r_{tt}, respectively. The branch-cut (radiation continuum) contribution is

$$G_{r,yy}^{\mathrm{bc}} = \frac{-j}{8\pi}\int_{\Gamma_{bc}}\left(\frac{r_{tt}h_{tt}}{k_z} - \frac{r_{pp}k_zh_{pp}}{k^2}\right)k_Te^{-jk_z\left(z+z'\right)}dk_T. \tag{36}$$

IV. Examples and Results

In the following, we restrict attention to planar metallizations, for which $\chi_{ES}^{zz} = \chi_{MS}^{xx} = \chi_{MS}^{yy} = 0$. In this case, for the surface-susceptibility method, the coefficients r_{tt} and r_{pp} can be further simplified as

$$r_{tt} = \frac{-k^2\chi_{ES}^{xx} - k_T^2\chi_{MS}^{zz}}{k^2\chi_{ES}^{xx} + k_T^2\chi_{MS}^{zz} - 2jk_z} \tag{37}$$

$$r_{pp} = \frac{k_z\chi_{ES}^{xx}}{k_z\chi_{ES}^{xx} - 2j}. \tag{38}$$

A. Square Patch Array

Consider a suspended PEC periodic array of square patches with edge length l, gap between patches g, and period $p = l + g$, as shown in Fig. 2(a).

1) Susceptibility Analysis: The effective electric and magnetic polarizability densities for a square PEC patch array are $\alpha_{E,xx} = \alpha_{E,yy} = 1.02l^3$, $\alpha_{E,zz} = \alpha_{M,xx} = \alpha_{M,yy} = 0$, and $\alpha_{M,zz} = 0.4548l^3$ [32], [33], and from these, the components of the electric and magnetic surface-susceptibility dyadics can be analytically calculated in the sparse approximation [14]; see Appendix A. The vertical wavenumbers in air corresponding to the guided-wave poles (zeros of the reflection-coefficient denominators) are [2]

$$k_{z,tt} = \frac{-j \pm \sqrt{k^2\chi_{MS}^{zz}\left(\chi_{ES}^{xx} + \chi_{MS}^{zz}\right) - 1}}{\chi_{MS}^{zz}} \tag{39}$$

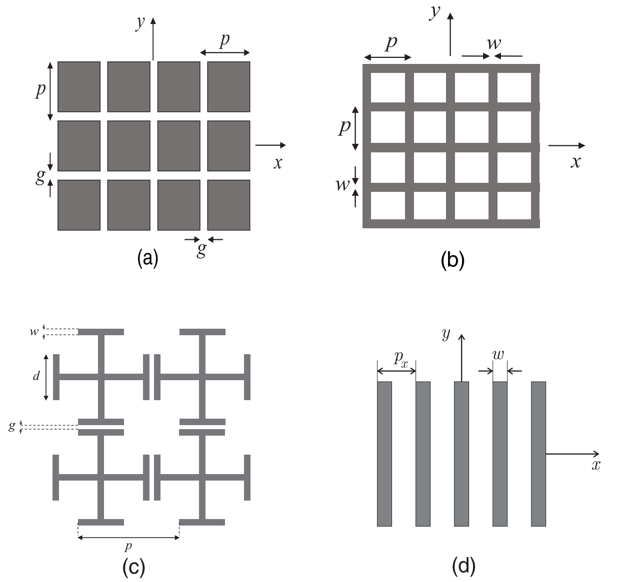

Fig. 2. (a) Square patch array. (b) Wire-mesh grid. (c) Jerusalem-cross array. (d) Strip array.

for r_{tt}, and

$$k_{z,pp} = \frac{2j}{\chi_{ES}^{xx}} \tag{40}$$

for r_{pp}. To generate a surface wave, one needs $\mathrm{Im}(k_z) < 0$ so that the wave is evanescent along the vertical (z) direction. For a square patch array, we have $\chi_{ES}^{xx} > 0$ and $\chi_{MS}^{zz} < 0$. Since for a VED source, only r_{pp} is involved in the calculation of the electric and magnetic fields, we can conclude that a VED source over a square patch array will not excite a surface wave (the surface is capacitive). For a HED, both r_{tt} and r_{pp} are needed in the field calculations, and so a HED over a square patch array will excite a surface wave if $\chi_{ES}^{xx} > -\chi_{MS}^{zz}$ (which is satisfied for a PEC square patch array), and the corresponding wavenumber is (39) with the minus sign chosen.

2) Surface-Impedance Analysis: The scalar equivalent grid impedances for TE and TM modes are [20], [25]

$$Z_g^{\mathrm{TE,patch}} = -j\frac{\eta}{2\alpha}\left[1 - \frac{k_T^2}{2k^2}\right]^{-1} \tag{41}$$

$$Z_g^{\mathrm{TM,patch}} = -j\frac{\eta}{2\alpha} \tag{42}$$

where $\alpha = \frac{kp}{\pi}\ln\left[\csc\left(\frac{\pi g}{2p}\right)\right]$. Then from (19), the pole of r_{pp} is

$$k_{z,pp} = j\frac{k}{\alpha}. \tag{43}$$

We always have $\alpha > 0$, and hence $\mathrm{Im}(k_{z,pp}) > 0$, so that the VED source excitation cannot support surface-wave propagation (as obtained above). The poles of r_{tt} are

$$k_{z,tt} = j\frac{k\left(1 \pm \sqrt{1+\alpha^2}\right)}{\alpha}. \tag{44}$$

Since $\alpha > 0$, only one solution (having the minus sign) satisfies the condition $\mathrm{Im}(k_z) < 0$, and this condition is always satisfied.

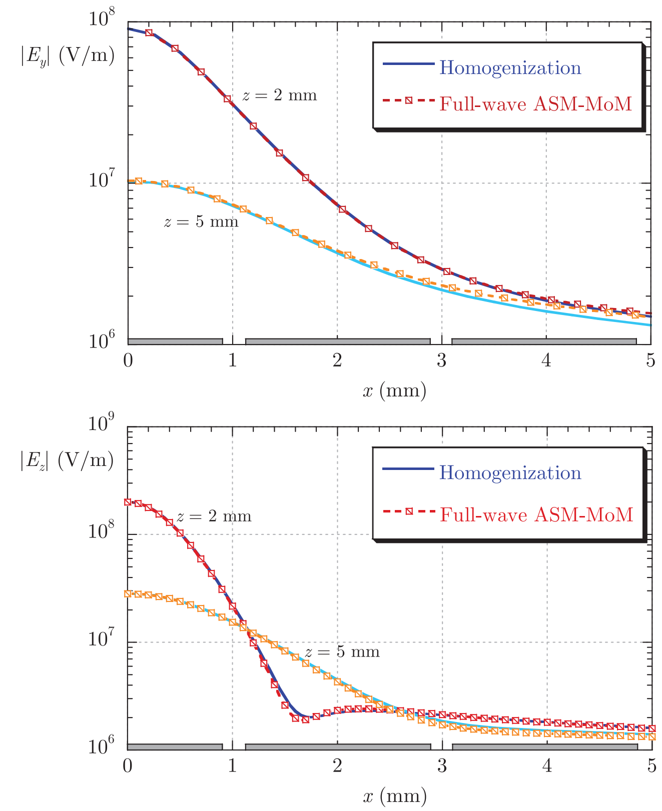

Fig. 3. Electric field excited by a 1-A HED (upper plot) or VED (lower plot) source above a square PEC patch array at $f = 15$ GHz, for $l = 1.8$ mm, $g = 0.2$ mm, $p = l + g = 2$ mm ($p/\lambda = 0.1$), $x' = 0$, $y' = 0$, $z' = 3$ mm, and $y = 0$.

That is to say, the HED source excitation can always support surface-wave propagation, as noted above.

As expected, the susceptibility method and the surface-impedance method lead to the same conclusion: the VED source excitation over a square PEC patch array cannot support surface-wave propagation, while the HED source excitation can always support surface-wave propagation. Considering the two methods (surface susceptibility and surface impedance), the surface-wave propagation constants will be equal if $k\chi_{ES}^{xx} = 2\alpha$, which is

$$\frac{1.02l^3}{p^2 - 1.02l^3/(2.78p)} \approx \frac{2p}{\pi}\ln\left[\csc\left(\frac{\pi(p-l)}{2p}\right)\right]. \tag{45}$$

Although these expressions appear quite different, it can be checked numerically that the expressions are approximately equal for a wide range of structural parameters.

We omit in the following a comparison of results using the susceptibility method and the surface-impedance method, although excellent agreement was found for $g \geq p/10$. For extremely dense arrays ($g < p/10$), the surface-impedance method yielded better results than the susceptibility method in comparisons with a full-wave array-scanning method (ASM, described below), although that is likely due to the fact that the patch polarizabilities were calculated assuming a sparse approximation. More accurate, numerically retrieved patch susceptibilities (either measured, or numerically computed, as described in [1], [14], and [18]) would be expected to restore

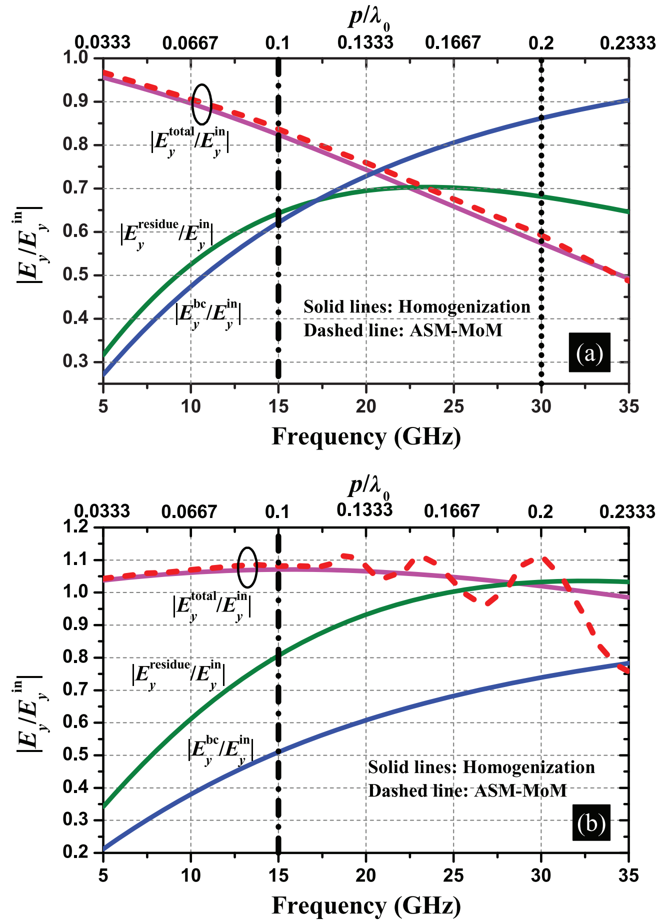

Fig. 4. Normalized total, residue, and bc E_y excited by a HED source above a square patch array. Structural parameters: $l = 1.8$ mm, $g = 0.2$ mm, $x' = y' = 0$, $x = y = \lambda_0/\sqrt{2}$, and (a) $z' = z = \lambda_0/5$; (b) $z' = z = \lambda_0/10$. (The vertical dashed-dotted line represents the homogenization condition $p/\lambda_0 = 0.1$, and the vertical dotted line represents the condition $z = p$. These two vertical lines overlap in Fig. 4(b). The vertical lines in the later figures have the same meaning).

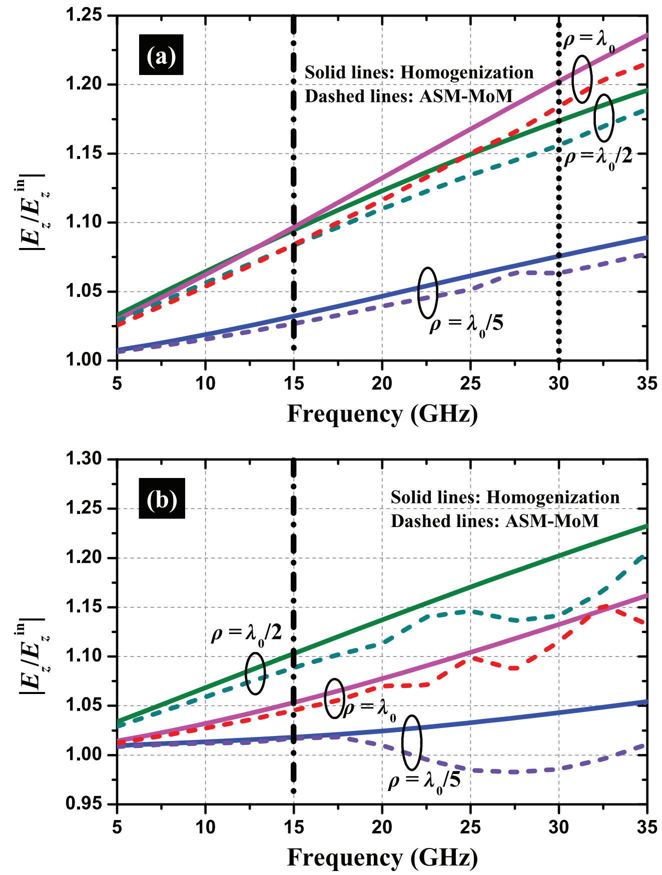

Fig. 5. z-component of electric field (normalized to the incident field) excited by a VED source above a square patch array. Parameters: $l = 1.8$ mm, $g = 0.2$ mm, $x' = y' = 0$, $x = y = \rho/\sqrt{2}$. (a) $z' = z = \lambda_0/5$ and (b) $z' = z = \lambda_0/10$.

accuracy to the susceptibility method for dense arrays of patches. In the following figures, we make comparisons to results obtained using the full-wave ASM [27], [28], which can be considered to yield the exact (up to numerical accuracy) result.

Fig. 3 shows the electric field spatial profile (as a function of x) over several periods of a square PEC patch array for HED and VED excitation. Excellent agreement is observed between the proposed homogenized method and full-wave ASM-MoM.

Fig. 4 shows the amplitude of the total, residue, and branch-cut E_y fields (normalized to the direct source-excited field without the metasurface, denoted as E_y^{in}) versus frequency for a HED source excitation. The representation in terms of such normalized fields has been chosen to outline and quantify the effects of the metasurface on the source radiation. As one expects, when the source and observation points move closer to the surface [from $z' = z = \lambda_0/5$ in Fig. 4(a) to $z' = z = \lambda_0/10$ in Fig. 4(b)], the residue field (surface wave) is enhanced, while the branch-cut field (radiation wave) decreases. Moreover, both the residue field and branch-cut field contribute significantly to the total field. The vertical dashed-dotted line represents a reasonable condition for the validity of homogenization, $p/\lambda_0 = 0.1$. Comparison with the ASM shows that indeed excellent results are found in this case (to the left of the vertical dashed-dotted line). The vertical dotted line represents the condition $z = p$ (since we set $z' = z \propto \lambda_0$, z is decreasing as frequency increases); to the left of this line $z > p$, which we found to be a reasonable condition for approximate validity of the homogenized Green's functions in the near field [25]. For Fig. 4(a), this is simply shown for reference, since it lies to the right of the dashed-dotted vertical line, and thus lies in a region where the homogenization condition is already violated. For Fig. 4(b), the dashed-dotted and dotted vertical lines overlap.

Fig. 5 shows the normalized z-component of electric field excited by a VED source above a square PEC patch array. Since no surface wave is excited, we only show the total normalized field (equal to unity plus the branch-cut contribution). Good agreement with the ASM results is again found in the validity regime (left of the solid dashed-dotted vertical line). The region to the right of the dashed-dotted vertical line is included merely to demonstrate the breakdown of homogenization.

Fig. 6 shows the z- and y-components of the far fields calculated from the homogenization model (with the method of

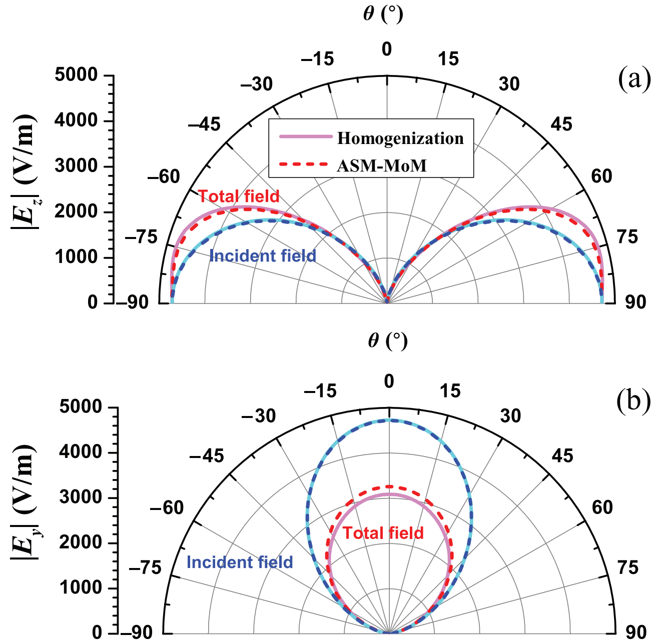

Fig. 6. Far field above a square patch array (solid lines: homogenization model; dashed lines: ASM-MoM). Structural parameters: $l = 1.8$ mm, $g = 0.2$ mm, $x' = y' = 0$, $r = 100\lambda_0$, $z = r\cos\theta$, $f = 15$ GHz. (a) E_z in the xOz plane excited by a VED source, $z' = 3p$, $x = r\sin\theta$, $y = 0$. (b) E_y in the yOz plane excited by a HED source, $z' = p$, $x = 0$, $y = r\sin\theta$.

stationary phase as shown in Appendix B) and from the full-wave ASM-MoM method. Good agreement between these two methods is obtained for both VED and HED dipole excitations.

B. Wire-Mesh Grid

The wire-mesh grid is the complementary configuration of the PEC patch array, as shown in Fig. 2(b). The surface-impedance parameters can be calculated as [20]

$$Z_g^{TE} = j\frac{\eta}{2}\alpha \tag{46}$$

$$Z_g^{TM} = j\frac{\eta}{2}\alpha\left(1 - \frac{k_T^2}{2k^2}\right) \tag{47}$$

where $\alpha = \frac{kp}{\pi}\ln\left[\csc\left(\frac{\pi w}{2p}\right)\right]$. Unlike the patch array, in the wire mesh grid, the VED source excitation can always support surface-wave propagation (as can the HED source). The pole of r_{pp} supporting surface wave is

$$k_{z,pp} = j\frac{k\left(1 - \sqrt{1+\alpha^2}\right)}{\alpha}. \tag{48}$$

Fig. 7 shows the normalized field E_y excited by a HED source above a wire-mesh grid. Again, good agreement is found with the ASM results when homogenization is valid (left of the solid line).

C. Jerusalem-Cross Array

For the Jerusalem-Cross (JC) array [shown in Fig. 2(c)], it seems there is no susceptibility model in the literature, although

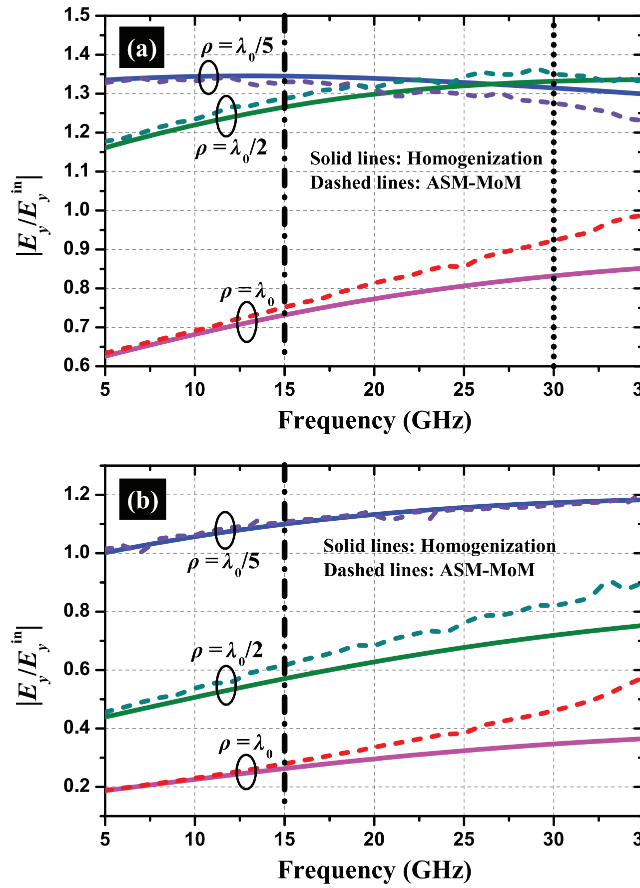

Fig. 7. Normalized E_y excited by a HED source above a wire-mesh grid. Structural parameters: $p = 2$ mm, $w = 0.2$ mm, $x' = y' = 0$, $x = y = \rho/\sqrt{2}$. (a) $z' = z = \lambda_0/5$ and (b) $z' = z = \lambda_0/10$.

the surface impedances for the TE and TM modes, i.e., Z_g^{TE} and Z_g^{TM}, can be found in [25] and references therein. The poles of r_{pp} lead to

$$k_{z,pp} = j\frac{2\varepsilon_0 - k\alpha C_g}{C_g} \tag{49}$$

with the JC capacitance C_g given in [25]. To have a surface wave, one needs $\mathrm{Im}(k_z) < 0$, i.e., frequency $f > f_c$, where f_c depends on the geometrical parameters. The analytical solutions for the poles of r_{tt} are quite complicated (involving the solution of a cubic equation) and are not discussed here.

For the JC array, Fig. 8 shows the electric field as a function of x for HED and VED excitation. Good agreement between the two methods is observed.

Fig. 9 shows the normalized total, residue, and branch-cut E_z fields versus frequency for the VED source excitation, and Fig. 10 shows the normalized E_y fields excited by the HED source. Agreement with the ASM results is again found to be good in the homogenization regime. Fig. 11 shows the far field due to a source over a JC array, where it is seen that the presence of the array significantly affects the far field.

Regarding computation time, it should be noted that for the near fields, the homogenized Green's function computations require the computation of 1-D Sommerfeld integrals, which can be done in seconds, whereas the ASM method takes, on a

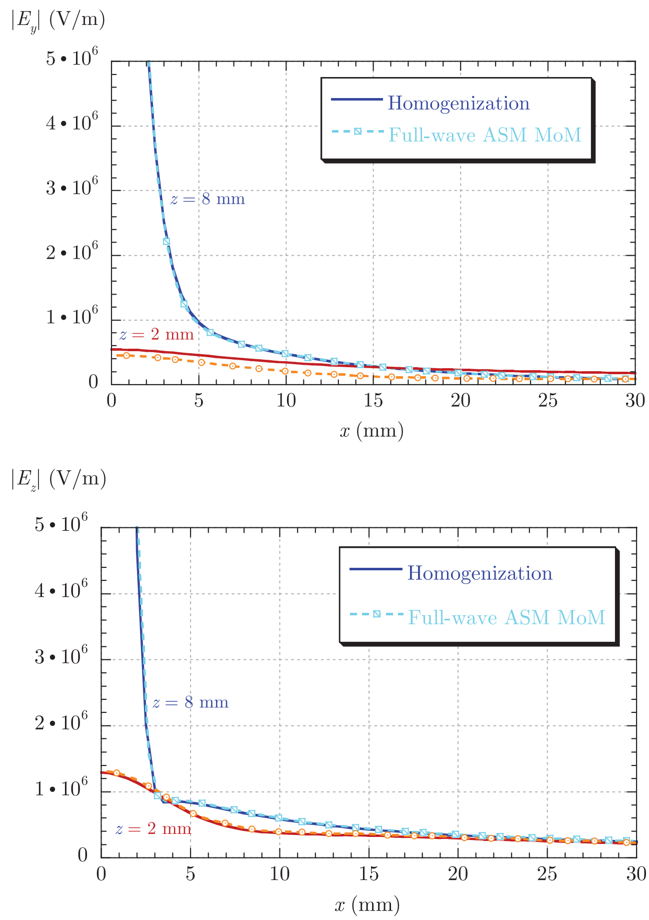

Fig. 8. Electric field excited by a 1-Amp HED (upper plot) or VED (lower plot) source above a JC array at $f = 10$GHz, for $p = 4.3$ mm, $g = 0.1$ mm, $d = 2.8$ mm, $w = t = 0.2$ mm, $x' = 0$, $y' = 0$, $z' = 10$ mm, and $y = 0$.

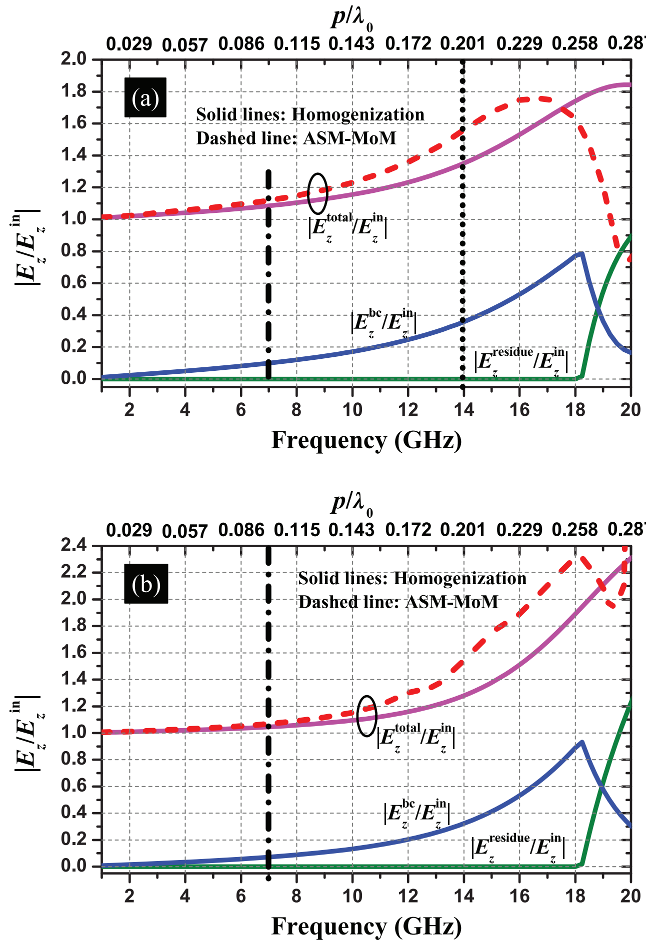

Fig. 9. Normalized total, residue, and bc E_z excited by VED source above a JC array. Structural parameters: $p = 4.3$ mm, $g = 0.1$ mm, $d = 2.8$ mm, $w = t = 0.2$ mm, $x' = y' = 0$, $x = y = \lambda_0/\sqrt{2}$. (a) $z' = z = \lambda_0/5$ and (b) $z' = z = \lambda_0/10$.

similar computer, several minutes or hours per frequency point, depending on the mesh of the PEC objects and if symmetry considerations can be applied [28].

D. Strip Grid Array

The strip array configuration shown in Fig. 2(d), if made of graphene, allows controlled excitation of surface waves in the THz regime, as will be shown in this section. Note that the previous three examples were isotropic, wherein the Green's function could be computed using the integrals provided in Section III. The graphene strip array is an anisotropic surface, and hence, the Green's function must be computed as a 2-D integral. The in-plane effective conductivity tensor of the proposed structure can be analytically obtained using an effective medium theory [36]. The dispersion topology of the proposed structure may range from elliptical to hyperbolic as a function of its geometrical and electrical parameters. The homogenized conductivity is $\underline{\boldsymbol{\sigma}}_e = \hat{\mathbf{x}}\hat{\mathbf{x}}\sigma_{xx} + \hat{\mathbf{y}}\hat{\mathbf{y}}\sigma_{yy}$, where

$$\sigma_{yy} = \sigma\frac{w}{p_x} \text{ and } \sigma_{xx} = \frac{p_x\sigma\sigma_c}{w\sigma_c + g\sigma} \tag{50}$$

where p_x and w are the periodicity and width of the strips, respectively, $g = p_x - w$ is the separation between two consecutive strips, σ is the 2-D conductivity, and $\sigma_c = j\frac{\omega\epsilon_0 p_x}{\pi}\ln(\csc\frac{\pi g}{2p_x})$ is an equivalent conductivity associated with the near-field coupling between adjacent strips.

Fig. 12 shows the normalized scattered electric field for the VED source excitation at $f = 10$ GHz versus angle ϕ for $\rho = 0.2\lambda$ for PEC strips having width $w = 3$ mm, period $p_x = 3.5$ mm ($p_x/\lambda = 0.117$), and height $z = z' = \lambda/5$ ($z/p_x = z'/p_x = 1.713$). In this case, $\sigma_{yy} \to \infty$ and $\sigma_{xx} \simeq \frac{p_x}{g}\sigma_c = j6.51$ mS). The field near the surface is almost isotropic, due to the large value of strip conductivities. In fact, 2D conductivity values larger in magnitude than approximately 0.1 yield essentially PEC behavior (consider, e.g., that a good metal at low GHz frequencies can typically be considered a PEC, and that the equivalent 2D conductivity is $\sigma_{2D} = \sigma_{3D}t$, where t is metal thickness. Given $\sigma_{3D} \approx 10^7$ S/m, and, say, $t = 10$ nm, then $\sigma_{2D} \approx 0.1$ nmS). There is some disagreement in magnitude between homogenized and ASM results, but the field pattern is the same.

To obtain a directional response, the strip conductivity needs to be reduced in an appropriate manner. For this application, graphene represents a useful material since its relaxation time is of the order of ps, so that the desired conductivity response can

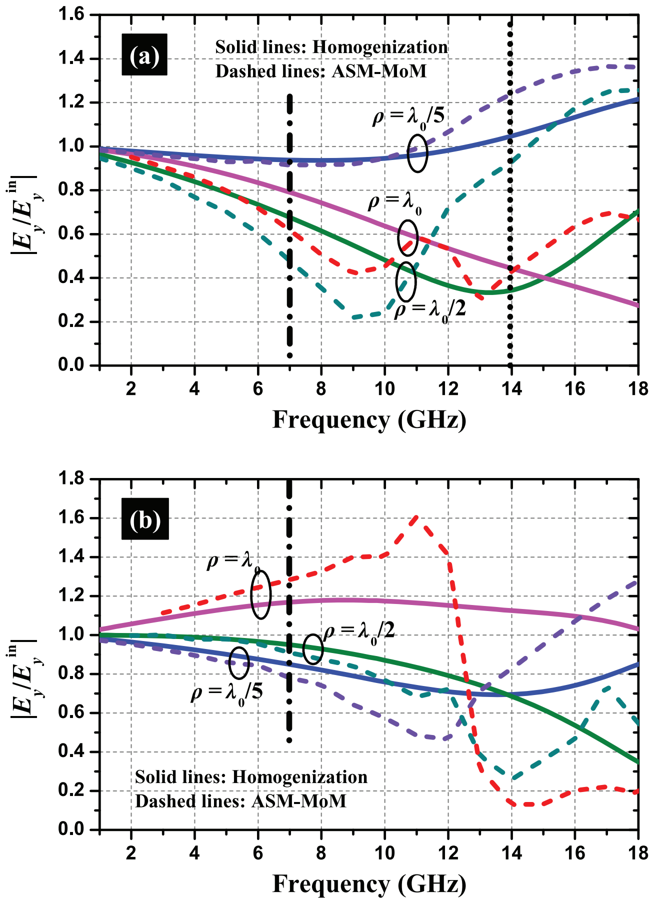

Fig. 10. Normalized E_y excited by HED source above a JC array. Structural parameters: $p = 4.3$ mm, $g = 0.1$ mm, $d = 2.8$ mm, $w = t = 0.2$ mm, $x' = y' = 0$, $x = y = \rho/\sqrt{2}$. (a) $z' = z = \lambda_0/5$ and (b) $z' = z = \lambda_0/10$.

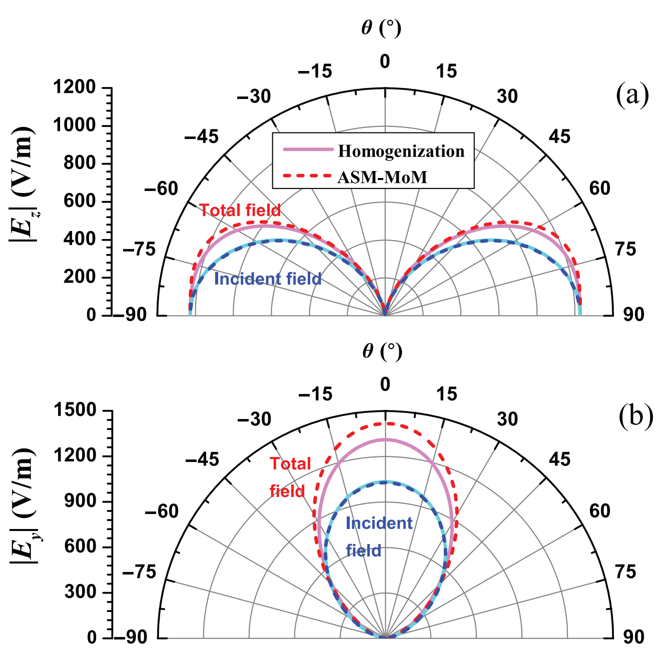

Fig. 11. Far field above a JC array (solid lines: homogenization model; dashed lines: ASM-MoM). Structural parameters: $p = 4.3$ mm, $g = 0.1$ mm, $d = 2.8$ mm, $w = t = 0.2$ mm, $x' = y' = 0$, $r = 100\lambda_0$, $z = r\cos\theta$, $f = 7$ GHz. (a) E_z in the xOz plane excited by a VED source, $z' = 2p$, $x = r\sin\theta$, $y = 0$. (b) E_y in the yOz plane excited by a HED source, $z' = 3p$, $x = 0$, $y = r\sin\theta$.

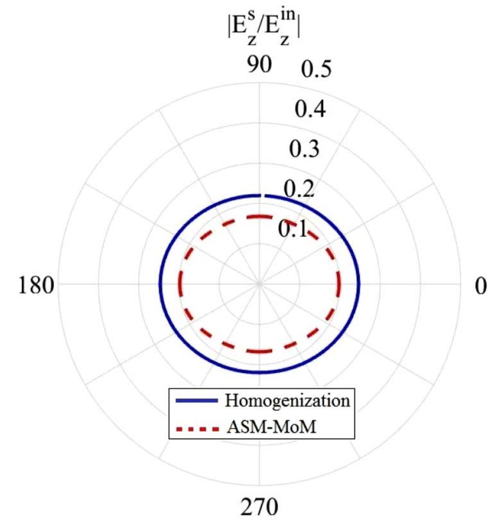

Fig. 12. Normalized scattered electric field excited by a VED source at $f = 10$ GHz versus angle ϕ for $\rho = 0.2\lambda$ for PEC strips having width $w = 3$ mm, period $p_x = 3.5$ mm ($p_x/\lambda = 0.117$) and height $z = z' = \lambda/5$ ($z/p_x = z'/p_x = 1.713$). Solid blue line shows homogenized results and dashed red line shows ASM results.

be obtained in the THz range (for metals, the desired response would be in the visible). Moreover, graphene is tunable via an external bias, such that the strip-array effective conductivity is tunable [36]. Fig. 13 shows the reflected/scattered electric field for the VED source excitation as a function of angle for $\rho = 0.2\lambda$ when the strips consist of seven-layer thick graphene at room temperature, with width $w = 196$ nm, period $p_x = 200$ nm, and $f = 10$ THz ($p_x/\lambda = 0.0067$). Graphene relaxation time is 0.35 ps (for graphene conductivity, see [37]), and $z = z' = \lambda/50$ ($z/p_x = z'/p_x = 3$). The graphene is biased using two values of chemical potential μ_c, and it can be seen that this hyperbolic surface provides tunable and highly directional surface-wave propagation.

V. Conclusion

A homogenized electric-dipole-source Green's function model for anisotropic metasurface structures has been presented. The method is very efficient compared to full-wave solvers, and leads to physical insight into the wave dynamics. The calculated results are compared to a full-wave method, and good agreement is obtained when homogenization is valid, except when field points are too close to the metasurface ($z < p$). As a final remark, although the method has been presented for uniform metasurfaces, it should be mentioned that homogenized representations of nonuniform metasurfaces (such as those used in [9], [12], [13], [38]) are also possible, under the adiabatic assumption that the length scale of variation of the involved susceptibilities or surface impedances is large with respect to the local microscopic periodicity. In particular, the resulting nonuniform impedance boundary condition can be used to formulate a boundary integral equation that can then be discretized numerically with the method of moments. The main difficulty in this case would arise from the dependence of the local surface impedance on the wavenumbers (i.e., from its spatially dispersive nature). A general solution to this issue

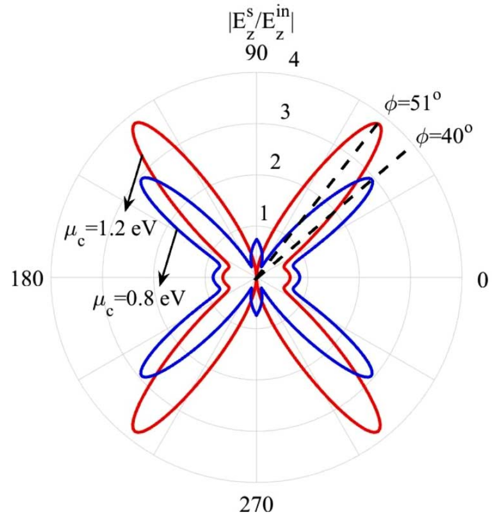

Fig. 13. Normalized scattered electric field excited by a VED source for graphene strip array with $w = 196$ nm, $p_x = 200$ nm, and $f = 10$ THz. Two bias values are considered, $\mu_c = 0.8$ eV, leading to $\sigma_{xx} = 0.8637 + j14.2337$ mS and $\sigma_{yy} = 0.4666 - j10.2604$ mS, and $\mu_c = 1.2$ eV, $\sigma_{xx} = 0.2766 + j9.8801$ mS and $\sigma_{yy} = 0.6999 - j15.3907$ mS.

is not yet available, as far as we know; however, approximate approaches have been proposed in the literature, based on, e.g., evaluating the surface impedance at a fixed wavenumber (that of a locally dominant surface or leaky wave [39]) or introducing a rational approximation of the surface impedance that translates into an integro-differential boundary condition amenable to discretization [40].

Appendix A
Relation Between Susceptibility and Polarizability

The relations between the electric/magnetic susceptibilities and polarizabilities are [14]

$$\chi_{ES}^{tt} = \frac{N\langle\alpha_{E,tt}\rangle}{1 - N\langle\alpha_{E,tt}\rangle/(4r)} \tag{51}$$

$$\chi_{ES}^{zz} = \frac{N\langle\alpha_{E,zz}\rangle}{1 + N\langle\alpha_{E,zz}\rangle/(2r)} \tag{52}$$

$$\chi_{MS}^{tt} = \frac{-N\langle\alpha_{M,tt}\rangle}{1 + N\langle\alpha_{M,tt}\rangle/(4r)} \tag{53}$$

$$\chi_{MS}^{zz} = \frac{-N\langle\alpha_{M,zz}\rangle}{1 - N\langle\alpha_{M,zz}\rangle/(2r)} \tag{54}$$

where tt in (51) and (53) represents xx or yy, α_E and α_M are the electric and magnetic polarizabilities of an individual element, N is the number of elements per unit area ($N = 1/p^2$ for square array with period of p), the symbol $<>$ represents an average over the elements, and r is a constant depending on the array structure ($r = 0.6956p$ for square array).

Appendix B
Far Field by Method of Stationary Phase

For the far fields, the Sommerfeld integrals can be calculated totally analytically with the method of stationary phase as follows:

$$\begin{aligned} G_{r,zz} &= \frac{1}{8\pi}\int_{-\infty}^{\infty}\frac{r_{pp}k_T^3}{k^2\sqrt{k_T^2-k^2}}H_0^{(2)}(k_T\rho)e^{-\sqrt{k_T^2-k^2}(z+z')}dk_T \\ &\approx \frac{r_{pp}e^{-jkr}\sin^2\theta}{4\pi r} \end{aligned} \tag{55}$$

$$\begin{aligned} G_{r,yy} &= \frac{-j}{8\pi}\int_{-\infty}^{\infty}\left(\frac{r_{tt}h_{tt}}{k_z} - \frac{r_{pp}k_z h_{pp}}{k^2}\right)k_T e^{-jk_z(z+z')}dk_T \\ &\approx \frac{1}{4\pi r}\cos\theta e^{-jkr}\left(\frac{r_{tt}h'_{tt}}{\cos\theta} - r_{pp}h'_{pp}\cos\theta\right) \end{aligned} \tag{56}$$

where $h'_{tt} = \frac{j(\sin^2\phi - \cos^2\phi)}{kr\sin^2\theta} + \cos^2\phi$, $h'_{pp} = \frac{j(\cos^2\phi - \sin^2\phi)}{kr\sin^2\theta} + \sin^2\phi$, $z + z' = r\cos\theta$, $\rho = r\sin\theta$, and $H_0^{(2)}(k_T\rho) \approx \sqrt{\frac{2}{\pi k_T\rho}}e^{-j(k_T\rho - \pi/4)}$ are applied.

References

[1] C. L. Holloway, E. F. Kuester, J. A. Gordon, J. O'Hara, J. Booth, and D. R. Smith, "An overview of the theory and applications of metasurfaces: The two-dimensional equivalents of metamaterials," *IEEE Antennas Propag. Mag.*, vol. 54, no. 2, pp. 10–35, Apr. 2012.

[2] C. L. Holloway, D. C. Love, E. F. Kuester, J. A. Gordon, and D. A. Hill, "Use of generalized sheet transition conditions to model guided waves on metasurfaces/metafilms," *IEEE Trans. Antennas Propag.*, vol. 60, no. 11, pp. 5173–5186, Nov. 2012.

[3] N. Meinzer, W. L. Barnes, and I. R. Hooper, "Plasmonic meta-atoms and metasurfaces," *Nat. Photonics*, vol. 8, no. 12, pp. 889–898, 2014.

[4] A. Fallahi and J. Perruisseau-Carrier, "Design of tunable biperiodic graphene metasurfaces," *Phys. Rev. B*, vol. 86, no. 19, p. 195408, 2012.

[5] Y. R. Padooru, A. B. Yakovlev, C. S. Kaipa, G. W. Hanson, F. Medina, and F. Mesa, "Dual capacitive-inductive nature of periodic graphene patches: Transmission characteristics at low-terahertz frequencies," *Phys. Rev. B*, vol. 87, no. 11, p. 115401, 2013.

[6] A. V. Kildishev, A. Boltasseva, and V. M. Shalaev, "Planar photonics with metasurfaces," *Science*, vol. 339, no. 6125, p. 1232009, 2013.

[7] N. Yu and F. Capasso, "Flat optics with designer metasurfaces," *Nat. Mater.*, vol. 13, no. 2, pp. 139–150, 2014.

[8] Y. Zhao, N. Engheta, and A. Alù, "Homogenization of plasmonic metasurfaces modeled as transmission-line loads," *Metamaterials*, vol. 5, no. 2, pp. 90–96, 2011.

[9] M. A. Salem and C. Caloz, "Manipulating light at distance by a metasurface using momentum transformation," *Opt. Express*, vol. 22, no. 12, pp. 14530–14543, 2014.

[10] Y. Zhao and A. Alù, "Manipulating light polarization with ultrathin plasmonic metasurfaces," *Phys. Rev. B*, vol. 84, no. 20, p. 205428, 2011.

[11] D. F. Sievenpiper, J. H. Schaffner, H. J. Song, R. Y. Loo, and G. Tangonan, "Two-dimensional beam steering using an electrically tunable impedance surface," *IEEE Trans. Antennas Propag.*, vol. 51, no. 10, pp. 2713–2722, Oct. 2003.

[12] C. Pfeiffer and A. Grbic, "Metamaterial Huygens surfaces: Tailoring wave fronts with reflectionless sheets," *Phys. Rev. Lett.*, vol. 110, no. 19, p. 197401, 2013.

[13] A. Epstein and G. Eleftheriades, "Passive lossless Huygens metasurfaces for conversion of arbitrary source field to directive radiation," *IEEE Trans. Antennas Propag.*, vol. 32, no. 11, pp. 5680–5695, Nov. 2014.

[14] C. L. Holloway, A. Dienstfrey, E. F. Kuester, J. F. O'Hara, A. K. Azad, and A. J. Taylor, "A discussion on the interpretation and characterization of metafilms/metasurfaces: The two-dimensional equivalent of metamaterials," *Metamaterials*, vol. 3, no. 2, pp. 100–112, 2009.

[15] E. F. Kuester, M. A. Mohamed, M. Piket-May, and C. L. Holloway, "Averaged transition conditions for electromagnetic fields at a metafilm," *IEEE Trans. Antennas Propag.*, vol. 51, no. 10, pp. 2641–2651, Oct. 2003.

[16] C. L. Holloway, M. A. Mohamed, E. F. Kuester, and A. Dienstfrey, "Reflection and transmission properties of a metafilm: With an application to a controllable surface composed of resonant particles," *IEEE Trans. Electromagn. Compat.*, vol. 47, no. 4, pp. 853–865, Nov. 2005.

[17] C. L. Holloway, E. F. Kuester, and D. Novotny, "Waveguides composed of metafilms/metasurfaces: The two-dimensional equivalent of metamaterials," *IEEE Antennas Wireless Propag. Lett.*, vol. 8, pp. 525–529, Mar. 2009.

[18] C. L. Holloway, E. F. Kuester, and A. Dienstfrey, "Characterizing metasurfaces/metafilms: The connection between surface susceptibilities and effective material properties," *IEEE Antennas Wireless Propag. Lett.*, vol. 10, pp. 1507–1511, Jan. 2011.
[19] S. Tretyakov, *Analytical Modeling in Applied Electromagnetics*. Norwood, MA, USA: Artech House, 2003.
[20] O. Luukkonen *et al.*, "Simple and accurate analytical model of planar grids and high-impedance surfaces comprising metal strips or patches," *IEEE Trans. Antennas Propag.*, vol. 56, no. 6, pp. 1624–1632, Jun. 2008.
[21] C. S. Kaipa, A. B. Yakovlev, F. Medina, F. Mesa, C. A. Butler, and A. P. Hibbins, "Circuit modeling of the transmissivity of stacked two-dimensional metallic meshes," *Opt. Express*, vol. 18, no. 13, pp. 13309–13320, 2010.
[22] C. S. Kaipa, A. B. Yakovlev, F. Medina, and F. Mesa, "Transmission through stacked 2D periodic distributions of square conducting patches," *J. Appl. Phys.*, vol. 112, no. 3, p. 033101, 2012.
[23] Y. R. Padooru, A. B. Yakovlev, P.-Y. Chen, and A. Alù, "Analytical modeling of conformal mantle cloaks for cylindrical objects using sub-wavelength printed and slotted arrays," *J. Appl. Phys.*, vol. 112, no. 3, p. 034907, 2012.
[24] P.-Y. Chen, J. Soric, Y. R. Padooru, H. M. Bernety, A. B. Yakovlev, and A. Alù, "Nanostructured graphene metasurface for tunable terahertz cloaking," *New J. Phys.*, vol. 15, no. 12, p. 123029, 2013.
[25] S. Paulotto, P. Baccarelli, P. Burghignoli, G. Lovat, G. W. Hanson, and A. B. Yakovlev, "Homogenized Green's functions for an aperiodic line source over planar densely periodic artificial impedance surfaces," *IEEE Trans. Microw. Theory Techn.*, vol. 58, no. 7, pp. 1807–1817, Jul. 2010.
[26] G. Lovat, "Near-field shielding effectiveness of one-dimensional periodic planar screen with two-dimensional near-field sources," *IEEE Trans. Electromagn. Compt.*, vol. 51, no. 3, pp. 708–719, Aug. 2009.
[27] G. Lovat, R. Araneo, and S. Celozzi, "Dipole excitation of periodic metallic structures," *IEEE Trans. Antennas Propag.*, vol. 59, no. 6, pp. 2178–2189, Jun. 2011.
[28] R. Araneo, G. Lovat, and S. Celozzi, "Shielding effectiveness of periodic screens against finite high-impedance near-field sources," *IEEE Trans. Electromagn. Compat.*, vol. 53, no. 3, pp. 706–716, Aug. 2011.
[29] G. Lovat, R. Araneo, and S. Celozzi, "Electromagnetic shielding of resonant frequency-selective surfaces in the presence of dipole sources," *ACES J.*, vol. 29, pp. 442–450, 2014.
[30] S. K. Cho, *Electromagnetic Scattering*. Berlin, Germany: Springer-Verlag, 1990.
[31] G. W. Hanson, "Dyadic Green's functions for an anisotropic, non-local model of biased graphene," *IEEE Trans. Antennas Propag.*, vol. 56, no. 3, pp. 747–757, Mar. 2008.
[32] C. Holloway, D. Love, E. Kuester, A. Salandrino, and N. Engheta, "Sub-wavelength resonators: On the use of metafilms to overcome the $\lambda/2$ size limit," *IET Microw. Antennas Propag.*, vol. 2, no. 2, pp. 120–129, Mar. 2008.
[33] E. Arvas and R. F. Harrington, "Computation of the magnetic polarizability of conducting disks and the electric polarizability of apertures," *IEEE Trans. Antennas Propag.*, vol. 31, no. 5, pp. 719–725, Sep. 1983.
[34] C. L. Holloway and E. F. Kuester, "Equivalent boundary conditions for a perfectly conducting periodic surface with a cover layer," *Radio Sci.*, vol. 35, no. 3, pp. 661–681, 2000.
[35] A. Ishimaru, *Electromagnetic Wave Propagation, Radiation, and Scattering*. Englewood Cliffs, NJ, USA:Prentice-Hall, 1991.
[36] J. Sebastian Gomez-Diaz, M. Tymchenko, and A. Alù, "Hyperbolic plasmons and topological transitions over uniaxial metasurfaces," *Phys. Rev. Lett.*, vol. 114, p. 233901, 2015.
[37] G. W. Hanson, "Dyadic Green's functions and guided surface waves for a surface conductivity model of graphene," *J. Appl. Phys.*, vol. 103, no. 6, p. 064302, 2008.
[38] G. Minatti *et al.*, "Modulated metasurface antennas for space: Synthesis, analysis and realizations," *IEEE Trans. Antennas Propag.*, vol. 63, no. 4, pp. 1288–1300, Apr. 2015.
[39] D. Di Ruscio, P. Burghignoli, P. Baccarelli, and A. Galli, "Omnidirectional radiation in the presence of homogenized metasurfaces," *Prog. Electromagn. Res.*, vol. 150, pp. 145–161, 2015.
[40] B. Stupfel and Y. Pion, "Impedance boundary conditions for finite planar and curved frequency selective surfaces," *IEEE Trans. Antennas Propag.*, vol. 53, no. 4, pp. 1415–1425, Apr. 2005.

Feng Liang was born in Hubei, China, in 1983. He received the B.S. degree in applied physics from the University of Electronic Science and Technology of China (UESTC), Chengdu, China, and the Ph.D. degree in electrical engineering from Wuhan University, Wuhan, China, in 2006 and 2011, respectively.

Since July 2011, he has been a Faculty Member of the School of Physical Electronics, UESTC, where he is now an Associate Professor. From April 2014 to March 2015, he was a Visiting Scholar at the Department of Electrical Engineering and Computer Science, University of Wisconsin-Milwaukee, Milwaukee, WI, USA. His research interests include theory, computation, and application of electromagnetic fields.

George W. Hanson (S'85–M'91–SM'98–F'09) was born in Glen Ridge, NJ, USA, in 1963. He received the B.S.E.E. degree from Lehigh University, Bethlehem, PA, USA, the M.S.E.E. degree from Southern Methodist University, Dallas, TX, USA, and the Ph.D. degree in electrical engineering from Michigan State University, East Lansing, MI, USA, in 1986, 1988, and 1991, respectively.

From 1986 to 1988, he was a Development Engineer with General Dynamics, Fort Worth, TX, USA, where he worked on radar simulators. From 1988 to 1991, he was a Research and Teaching Assistant with the Department of Electrical Engineering, Michigan State University. He is the coauthor of the book *Operator Theory for Electromagnetics: An Introduction* (Springer, 2002), and the author of *Fundamentals of Nanoelectronics* (Prentice-Hall, 2007). He is currently a Professor of Electrical Engineering and Computer Science with the University of Wisconsin-Milwaukee, Milwaukee, WI, USA. His research interests include nanoelectromagnetics, plasmonics, quantum optics, and mathematical methods in electromagnetics.

Dr. Hanson is a member of URSI Commission B, Sigma Xi, and Eta Kappa Nu, and was an Associate Editor for the IEEE TRANSACTIONS ON ANTENNAS AND PROPAGATION from 2002 to 2007. In 2006, he was the recipient of the S.A. Schelkunoff Best Paper Award from the IEEE Antennas and Propagation Society.

Alexander B. Yakovlev (S'94–M'97–SM'01) received the Ph.D. degree in radiophysics from the Institute of Radiophysics and Electronics, National Academy of Sciences, Kharkov, Ukraine, and the Ph.D. degree in electrical engineering from the University of Wisconsin-Milwaukee, Milwaukee, WI, USA, in 1992 and 1997, respectively.

In summer of 2000, he joined the Department of Electrical Engineering, University of Mississippi, Oxford, MS, USA, as an Assistant Professor and became an Associate Professor in 2004. Since July 2013, he has been a Full Professor of Electrical Engineering. He is a coauthor of the book *Operator Theory for Electromagnetics: An Introduction* (Springer, 2002). His research interests include mathematical methods in applied electromagnetics, homogenization theory, high-impedance surfaces for antenna applications, electromagnetic band-gap structures, metamaterial structures, wire media, graphene, cloaking, theory of leaky waves, transient fields in layered media, catastrophe, and bifurcation theories.

Dr. Yakovlev was an Associate Editor-in-Chief of the *ACES Journal* from 2003 to 2006, and was an Associate Editor of the IEEE TRANSACTIONS ON MICROWAVE THEORY AND TECHNIQUES from 2005 to 2008. He is a member of URSI Commission B. He was the recipient of the Young Scientist Award at the 1992 URSI International Symposium on Electromagnetic Theory, Sydney, Australia, and the Young Scientist Award at the 1996 International Symposium on Antennas and Propagation, Chiba, Japan. In 2003, the Junior Faculty Research Award at the School of Engineering, University of Mississippi, Oxford, MS, USA.

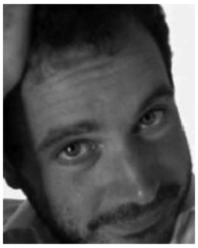

Giampiero Lovat (S'02–M'06) was born in Rome, Italy, on May 31, 1975. He received the Laurea degree (*cum laude*) in electronic engineering and the Ph.D. degree in applied electromagnetics both from "La Sapienza" University of Rome, Rome, Italy, in 2001 and 2005, respectively.

In 2005, he joined the Department of Electrical Engineering, "La Sapienza" University of Rome, Rome, Italy, and is currently an Assistant Professor with the same University. From January 2004 to July 2004, he was a Visiting Scholar at the University of Houston, Houston, TX, USA. He has coauthored the book *Electromagnetic Shielding* (IEEE-Wiley, 2008). He is a coauthor of *Fast Breaking Papers, October 2007* in EE and CS, about metamaterials [paper that had the highest percentage increase in citations in Essential Science Indicators, (ESI)]. His research interests include leaky waves, general theory and numerical methods for the analysis of periodic structures, electromagnetic shielding, and electrodynamics of graphene.

Dr. Lovat was the recipient of the Young Scientist Award from the 2005 URSI General Assembly, New Delhi, India, and in 2011, he was the recipient of the Best Paper Symposium Award at the 2011 IEEE EMC-S International Symposium on Electromagnetic Compatibility.

Paolo Burghignoli (S'97–M'01–SM'08) was born in Rome, Italy, on February 18, 1973. He received the Laurea degree (*cum laude*) in electronic engineering and the Ph.D. degree in applied electromagnetics from "La Sapienza" University of Rome, Rome, Italy, in 1997 and 2001, respectively.

In 1997, he joined the Department of Electronic Engineering, now Department of Information Engineering, Electronics and Telecommunications, "La Sapienza" University of Rome. From November 2010 to October 2015, he was an Assistant Professor with the same University. From January 2004 to July 2004, he was a Visiting Research Assistant Professor at the University of Houston, Houston, TX, USA. Since November 2015, he has been an Associate Professor with "La Sapienza" University of Rome. He is a coauthor of the *Fast Breaking Papers, October 2007* in EE and CS, about metamaterials [paper that had the highest percentage increase in citations in Essential Science Indicators, (ESI)]. His research interests include analysis and design of planar antennas and arrays, leakage phenomena in uniform and periodic structures, numerical methods for integral equations and periodic structures, propagation and radiation in metamaterials, and graphene electromagnetics.

Dr. Burghignoli was the recipient of the "Giorgio Barzilai" Laurea Prize (1996–1997) presented by the former IEEE Central and South Italy Section, of a 2003 IEEE MTT-S Graduate Fellowship, and of a 2005 Raj Mittra Travel Grant for Junior Researchers presented at the IEEE AP-S Symposium on Antennas and Propagation, Washington, DC, USA.

Rodolfo Araneo (SM'09) received the M.S. (*cum laude*) and Ph.D. degrees in electrical engineering from the University of Rome "La Sapienza", Rome, Italy, in 1999 and 2002, respectively.

In 1999, he was a Visiting Student at the National Institute of Standards and Technology (NIST), Boulder, CO, USA, where he was engaged in TEM cells and shielding. In 2000, he was a Visiting Researcher at the Department of Electrical and Computer Engineering, University of Missouri-Rolla (UMR), Rolla, MO, USA, where he was engaged in printed circuit boards and finite-difference time-domain techniques. He is currently an Associate Professor with the DIAEE at the same University. He has authored more than 130 papers in international journals and conference proceedings. He is the coauthor of the book *Electromagnetic Shielding* (IEEE-Wiley, 2008). He serves as a Reviewer for several international journals. His research interests include electromagnetic compatibility, energy harvesting and piezotronics based on piezoelectric ZnO nanostructures, and graphene electrodynamics, the development of numerical and analytical techniques for modeling high-speed printed circuit boards, shielding, transmission lines, periodic structures, devices based on graphene.

Dr. Araneo was the recipient of the Past Presidents Memorial Awards in 1999 from IEEE Electromagnetic Compatibility (EMC) Society and won the Best Conference Paper at the 2011 IEEE EMC Symposium.

Seyyed Ali Hassani Gangaraj (S'15) was born in Iran, in 1988. He received the B.Sc. and M.Sc. degrees from Iran University of Science and Technology (IUST), Tehran, Iran, all in electrical engineering in 2010 and 2012, respectively. He is currently pursuing the Ph.D. degree in electrical engineering at the University of Wisconsin-Milwaukee (UWM), Milwaukee, WI, USA.

He was a Research Assistant with the Microwave Engineering Research Laboratory, IUST, and currently is a Teaching Assistant with UWM. His research interests include fundamental electromagnetics, metamaterials, quantum optics, and quantum plasmonics.